FULL-LENGTH PAPER

THE PROTEIN SOCIETY WILEY

Structural basis of the inhibition of cystathionine γ-lyase from *Toxoplasma gondii* by propargylglycine and cysteine

Carmen Fernández-Rodríguez[1] | Carolina Conter[2] | Iker Oyenarte[1] | Filippo Favretto[2] | Iban Quintana[3] | Maria Luz Martinez-Chantar[1] | Alessandra Astegno[2] | Luis Alfonso Martínez-Cruz[1]

[1]Center for Cooperative Research in Biosciences (CIC bioGUNE), Basque Research and Technology Alliance (BRTA), Derio, Spain

[2]Department of Biotechnology, University of Verona, Verona, Italy

[3]TEKNIKER, Basque Research and Technology Alliance (BRTA), Eibar, Gipuzkoa, Spain

Correspondence
Alessandra Astegno, Department of Biotechnology, University of Verona, Strada Le Grazie 15, 37134 Verona, Italy.
Email: alessandra.astegno@univr.it

Luis Alfonso Martínez-Cruz, Center for Cooperative Research in Biosciences (CIC bioGUNE), Basque Research and Technology Alliance (BRTA), Bizkaia Technology Park, Building 801A, 48160 Derio, Spain.
Email: amartinez@cicbiogune.es

Review Editor: John Kuriyan

Abstract

Cystathionine γ-lyase (CGL) is a PLP-dependent enzyme that catalyzes the last step of the reverse transsulfuration route for endogenous cysteine biosynthesis. The canonical CGL-catalyzed process consists of an α,γ-elimination reaction that breaks down cystathionine into cysteine, α-ketobutyrate, and ammonia. In some species, the enzyme can alternatively use cysteine as a substrate, resulting in the production of hydrogen sulfide (H_2S). Importantly, inhibition of the enzyme and consequently of its H_2S production activity, makes multiresistant bacteria considerably more susceptible to antibiotics. Other organisms, such as *Toxoplasma gondii*, the causative agent of toxoplasmosis, encode a CGL enzyme (*Tg*CGL) that almost exclusively catalyzes the canonical process, with only minor reactivity to cysteine. Interestingly, the substitution of N360 by a serine (the equivalent amino acid residue in the human enzyme) at the active site changes the specificity of *Tg*CGL for the catalysis of cystathionine, resulting in an enzyme that can cleave both the CγS and the CβS bond of cystathionine. Based on these findings and to deepen the molecular basis underlying the enzyme-substrate specificity, we have elucidated the crystal structures of native *Tg*CGL and the variant *Tg*CGL-N360S from crystals grown in the presence of cystathionine, cysteine, and the inhibitor D,L-propargylglycine (PPG). Our structures reveal the binding mode of each molecule within the catalytic cavity and help explain the inhibitory behavior of cysteine and PPG. A specific inhibitory mechanism of *Tg*CGL by PPG is proposed.

Carmen Fernández-Rodríguez and Carolina Conter contributed equally to this work.

1 | INTRODUCTION

L-methionine (Met) and L-cysteine (Cys) can be interconverted via the intermediates L-homocysteine (HCys) and L-cystathionine (Cth) in the metabolic process known as transsulfuration. In terms of evolution, the transsulfuration pathway can operate in two opposite directions, that is, "*forward*" and "*reverse*." Forward transsulfuration is found in yeast, plants, and enteric bacteria and enables the formation of HCys from Cys. Reverse transsulfuration, on the other hand, allows for the synthesis of Cys from HCys, and is the only irreversible source of Cys in vertebrates. Reverse transsulfuration involves two consecutive steps catalyzed by two distinct enzymes. The first is cystathionine β-synthase (CBS; recently reviewed in González-Recio et al., n.d.), which catalyzes a β-replacement reaction in which the hydroxyl group of L-serine is replaced by HCys, yielding Cth and H_2O. The second is cystathionine γ-lyase (CGL), which facilitates the α,γ-elimination of Cth into Cys, α-ketobutyrate (KTB), and ammonia (Figure 1, reaction 1). Alternatively, CGL can act on atoms at the α and β positions of Cth to produce HCys, pyruvate, and ammonia (Figure 1, reaction 3). This latter reaction is known as the α,β-elimination, or β-lyase activity of CGL. In some organisms, CGL can also catalyze the formation of hydrogen sulfide (H_2S) using Cys and HCys as substrates (Figure 1, reactions 4 to 7). Noteworthy, such H_2S production is a critical metabolic process in the bacterial defense system. When the enzymes of the reverse transsulfuration are genetically disrupted, a wide range of bacterial pathogens known to be resistant to multiple antibiotics become sensitive to different classes of drugs and the host immune response (Mironov et al., 2017; Nzungize et al., 2019; Shatalin et al., 2011, 2021). This susceptibility offers new opportunities for antimicrobial strategy targeting pathogens like *Staphylococcus aureus* and *Pseudomonas aeruginosa*, which are pointed out as urgent targets by the World Health Organization (https://www.who.int/news/item/27-02-2017-who-publishes-list-of-bacteria-for-which-new-antibiotics-are-urgently-needed). An emerging body of research indicates that the benefit of inhibiting the enzymes of the reverse transsulfuration pathway and their H_2S-producing capacity can be extended to a broader range of plant, animal, and human pathogens, including organisms of the genus Apicomplexa like *Toxoplasma gondii*, the causative agent of toxoplasmosis, which is a worldwide spread infection that may have severe complications during pregnancy and in immunocompromised individuals (Wang et al., 2017).

We recently demonstrated that *T. gondii* encodes both the CBS (*Tg*CBS) and CGL (*Tg*CGL) enzymes of reverse transsulfuration (Conter et al., 2020, 2022; Fernández-Rodríguez et al., 2021; Maresi et al., 2018). *Tg*CGL (UniProtKB A0A125YN40, 46 kDa) shares a high amino acid identity with its homologs from Trypanosomes and Leishmania parasites (58% homology) but is less similar to the human and yeast counterparts (40% and 37% for *H. sapiens* and *S. cerevisiae*, respectively). Interestingly, *Tg*CGL almost exclusively catalyzes the α,γ-hydrolysis of Cth to yield Cys, KTB, and ammonia (Figure 1, reaction 1), with only minor reactivity for the hydrolysis of Cys to produce H_2S, pyruvate, and ammonia (Figure 1, reaction 4; Maresi et al., 2018). Some authors have proposed that the reaction specificity (α,γ- or α,β-elimination) of CGLs over Cth depends on the particular orientation adopted by Cth within the catalytic cavity (Messerschmidt et al., 2003). Concretely, it has been postulated that to form the external aldimine (first step of the catalysis) in the β-elimination process, the Cth molecule needs to be oriented with its sulfur atom in the γ position with respect to the PLP cofactor (Matoba et al., 2020). Instead, the γ-elimination requires the sulfur atom to be in the δ position with respect to PLP (Messerschmidt et al., 2003). Interestingly, some organisms such as *Lactobacillus plantarum* (Matoba et al., 2020), *Streptomyces phaechromogenes* (Nagasawa et al., 1984), and yeast (Hopwood et al., 2014) are capable of performing both γ- and β- carbon split showing CBL-like activity, thus suggesting wider available space for Cth to adopt either orientation.

It is interesting to note that *Tg*CGL also exhibits a product (Cys) inhibition (Maresi et al., 2018) by an unclear mechanism. Some authors suggest that the inhibitory effect is caused by a Cys-induced loss of the PLP cofactor at the catalytic cavity (Cherest et al., 1993; Sun et al., 2009). Others contend that the inhibition happens as a result of the formation of an external aldimine between Cys and PLP which is thought to transform into a thiazolidine adduct that prevents the reaction, as observed in human and yeast CGLs (Huang et al., 2010; Yamagata et al., 2002) as well as in other PLP-dependent enzymes (Kobylarz et al., 2016).

The differences in how certain CGL enzymes are inhibited highlight the need for more research into
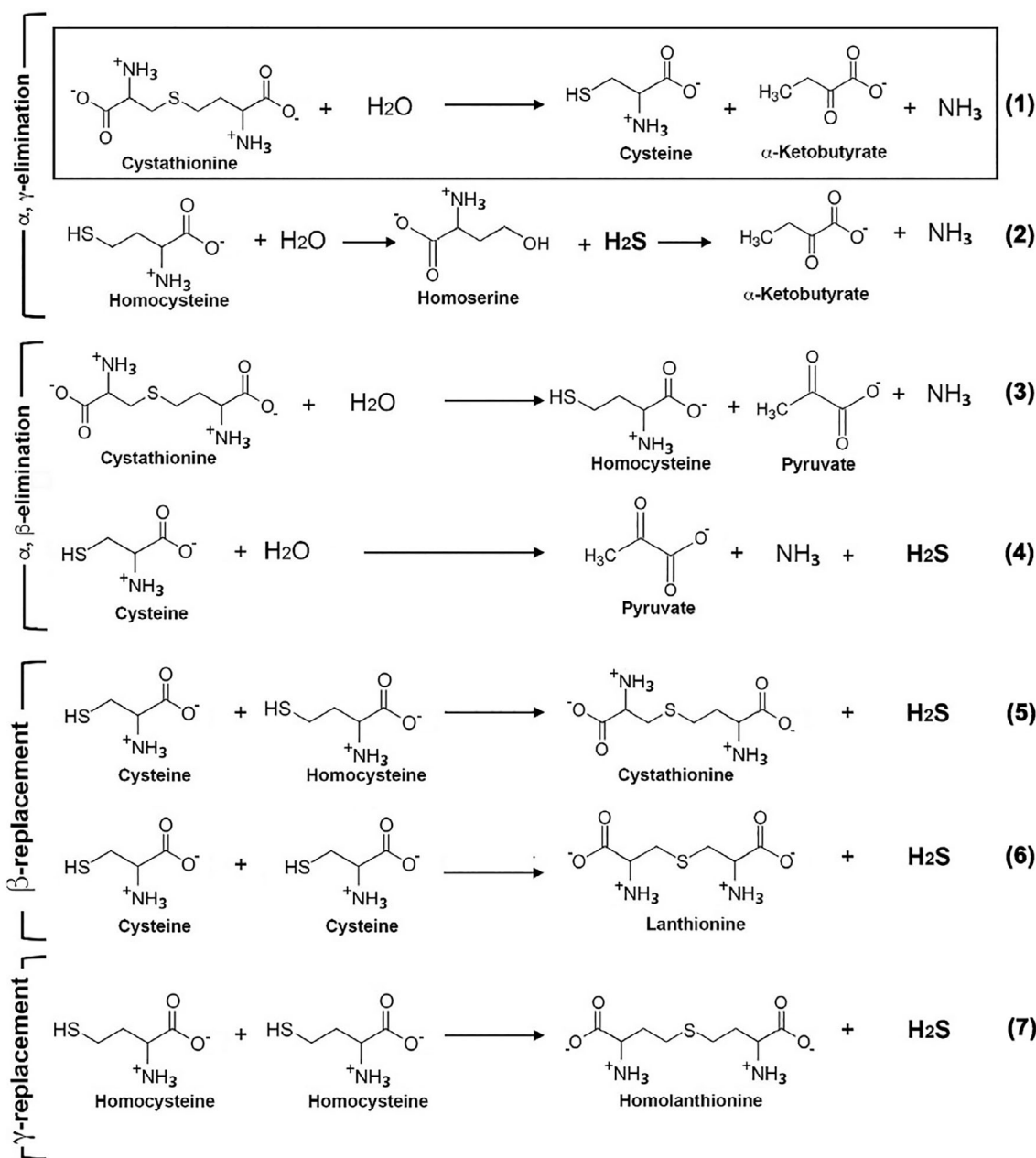
FIGURE 1 Scheme of reactions catalyzed by cystathionine γ-lyase. The canonical reaction (α,γ-elimination of Cth) is framed

specific protein–inhibitors interactions in pathogens and humans. The structural characterization of the corresponding protein–inhibitor complexes is a successful method for obtaining such information.

The domain architecture of CGL is remarkably conserved across species. Structurally, the protein belongs to the type I family of PLP-dependent enzymes, which also includes enzymes of the forward transsulfuration pathway (Messerschmidt et al., 2003), such as cystathionine γ-synthase (CGS) and cystathionine β-lyase (CBL). Most molecules designed to inhibit CGL enzymes are directed at the PLP molecule located at the catalytic site. For example, S-3-carboxypropyl-L-cysteine (CPC, a Cth analog lacking the α-amino group on the homocysteine side of the thioether) selectively and reversibly inhibits human CGL (HsCGL) and can act as a competitive inhibitor on both Cth and Cys cleavage reactions (Yadav et al., 2019). Co-crystallization of HsCGL with CPC yields an aminoacrylate intermediate (PDB ID 6NBA) that impedes the substrate to bind to PLP for enzymatic catalysis (Yadav et al., 2019). However, other compounds like D,L-propargylglycine (PPG), β-cyanoalanine, aminooxyacetic acid (AOAA), and L-aminoethoxyvinylglycine (AVG) function differently and inhibit the enzyme irreversibly by attacking the internal aldimine formed between the conserved lysine and PLP to form an

external aldimine (Asimakopoulou et al., 2013; Cramer et al., 2017; Lee et al., 2019; Matoba et al., 2020; Messerschmidt et al., 2003; Sagong et al., 2020; Sun et al., 2009; Wang et al., 2021).

In this study, we have characterized the three-dimensional structures of the wild-type TgCGL and its N360S variant from crystals grown in solutions containing Cth, Cys, and PPG. In addition to providing insights into the reaction specificity (α,γ- or α,β-elimination) of CGLs over Cth, our data explain the inhibitory effect of Cys on TgCGL and prompt us to postulate a specific mechanism for PPG's inhibition of TgCGL.

2 | RESULTS AND DISCUSSION

2.1 | Crystal structures of TgCGL variants alone and in the presence of the substrate Cth

Our previous studies revealed that the catalysis of TgCGL toward Cth is limited to the α,γ-elimination reaction, which yields Cys, KTB, and ammonia as final products (Figure 1, reaction 1). Of note, replacing N360 with serine, the equivalent amino acid residue in human enzyme, changes the reaction preference of the enzyme, which can now catalyze an α,β-elimination reaction toward Cth, yielding HCys, pyruvate, and ammonia (Figure 1, reaction 3; Maresi et al., 2018). These results suggested that the N360S substitution likely favors a Cth conformation suitable to undergo both γ- or β-eliminations (Maresi et al., 2018). To unravel this duality in catalytic activity, we elucidated the crystal structures of the wild-type TgCGL and its variant N360S alone and in the presence of the substrate Cth.

2.1.1 | Tg CGL and Tg CGL-N360S overall structures

The crystal structure of TgCGL was solved at a resolution ranging between 1.6 and 2.2 Å (Tables S1 and S2). TgCGL shows the overall fold of the type I family of PLP-dependent enzymes found in the CGLs from yeast, human, and bacteria. Each TgCGL protomer consists of three distinct regions (Figure 2a): (i) the N-terminal domain (residues 1–84) is composed of one helix (α1) and one long unstructured loop (residues 1–54) that interacts with the active site of its neighboring subunit in the dimer (e.g., loop from subunit A interacts with the PLP domain of subunit C). The first 20 residues of the N-domain are very flexible and barely interact with the bulk protein, explaining why they are not visible in the

electron density maps. (ii) The second region (residues 85–281), known as the "PLP-binding domain," represents the largest portion of the protein and houses the PLP cofactor covalently linked to the ε-amino group of a conserved lysine (K230), forming an internal aldimine. Structurally, this domain adopts an α/β/α fold, made up of seven β-strands (↑β1↓β7↑β6↑β5↑β4↑β2↑β3), mostly parallel, with strand β7 running antiparallel to the rest of the strands. Notably, the β-sheet is sandwiched between two helical bundles and is bent around helix α3. The first helical bundle includes four helices (α2, α5, α6, and α9), of which α5 and α6 are completely exposed to the solvent, whereas the other two, α2 and α9, play a key role in the dimer integrity by interacting with the short helix (α1) of the N-terminal domain, and helix α9 from the adjacent subunit (Figure 2a). In contrast with other organisms (e.g., yeast), TgCGL lacks a fifth helix (α7) inserted between α2 and α6, being this element laxer, and appearing as a loop that retains certain helicity between amino acid residues 216–221. At the opposite face of the β-sheet, the second bundle, formed by helices α3, α4, and α8, maintains interactions with the complementary dimer. (iii) The C-terminal domain (residues 282–417) is smaller and connected to the PLP domain through the long helix α10. This domain includes five α-helices (α10-α14) located on one side of a five-stranded β-sheet (↑β8↓β9↑β11↑β12), of which β10 is not visible in our TgCGL structure (Figure 2a).

Consistent with other CGLs, TgCGL exists as a homotetramer both in solution (as previously reported Maresi et al., 2018) and in the crystalline state (Figure 2b). The tetramer can be structurally described as a dimer of dimers with internal symmetry 222. The most compact association between neighboring molecules (analyzed using the PISA server; Krissinel & Henrick, n.d.) is that formed between monomers A-C (dimer-1) and B-D (dimer-2; Figure 2b). The buried surface area (BSA) for the A-C and B-D assemblies are 2405 and 2466 Å^2, respectively. The N-terminal domain from each subunit plays a key role in maintaining the integrity of each structural dimer by forming intermolecular hydrogen bonds, like those existing between the phosphate moiety of PLP and residues Y78 and R80 of the complementary monomer (Figure S1).

CGL enzymes are known to adopt open and closed conformations (Sun et al., 2009). The superimposition of the A-C TgCGL assembly with the human counterpart in the apo state (no PLP bound) revealed that the active site of apo HsCGL is considerably more expanded than that of TgCGL (rmsd = 2.968; Figures S2 and S3). The most significant differences reside in the α9, α10, and α12 helices and in the three loops H41-P84, T129- N137, and T228-Y232 (numbers corresponding to the TgCGL).
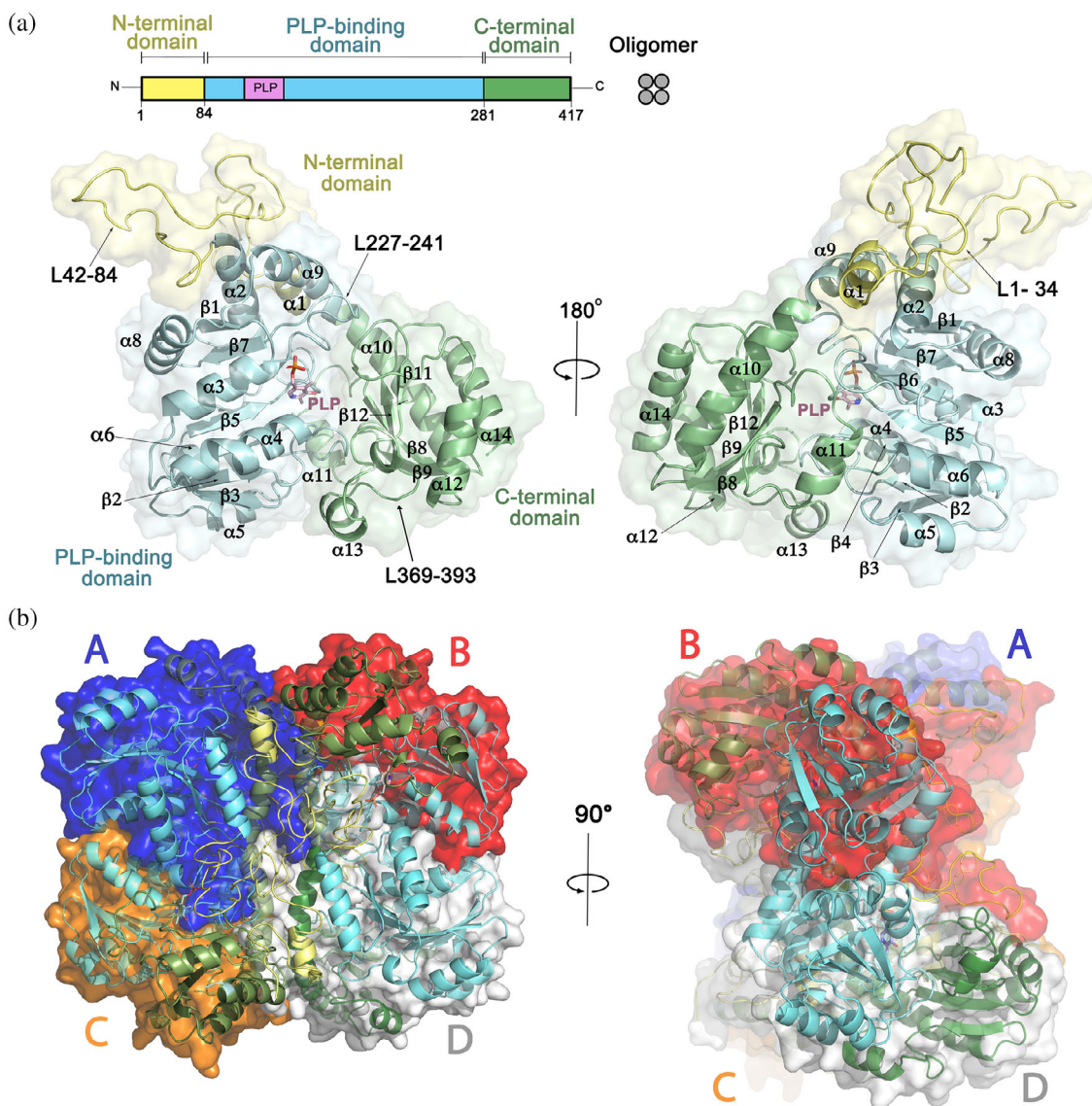
FIGURE 2 Crystal Structure of *Tg*CGL. (a) *Tg*CGL has a modular architecture consisting of three distinct domains: (i) N-terminal domain (yellow), (ii) PLP-binding domain (blue), and (iii) C-terminal domain (green). Ribbon representation of the *Tg*CGL monomer (secondary structure elements are labeled). Each color corresponds to the domain distribution described previously. (b) Tetrameric *Tg*CGL. The assembly can be structurally interpreted as two active dimers (dimer 1: subunits A (blue)-C (orange); dimer 2: subunits B (red)-D (gray)) related by a two-fold axis oriented vertically between the two dimers. The secondary elements from each subunit are colored according to the three distinct protein regions mentioned in Panel (a)

These loops are part of the walls of the catalytic site that harbors the PLP cofactor. The catalytic site includes two chambers made up of residues donated by the PLP-binding domain, the C-terminal segment of subunit A, and the N-terminal domain of subunit C. The PLP is located in chamber 1, as is commonly observed in most PLP-dependent enzymes (Figure 3a,b; Oliveira et al., 2011). Our crystals of native *Tg*CGL, revealed a co-crystallized molecule of TCEP that was present in the crystallization buffer (Figure 3b,c). Interestingly, TCEP occupies chamber 2 of the active site, which as described below, also represents the binding site of other molecules.

In *Tg*CGL, PLP is embedded by part of helix α3, strands of the PLP-binding domain (β5-β7), and of the C-terminal segment (β9, β11, and β12), and the connecting loops T129-G134, D205-P216, S227-G241, V351-I367, and Y58-P84 (the latter belongs to the complementary subunit of the structural dimer). Importantly, the aldehyde portion of PLP at position 4 is implicated in the formation of a Schiff base with the ε-amino group of lysine 230 (Figure 3c).

The overall fold of *Tg*CGL-N360S barely changes compared to the native enzyme (Figure S4). Superimposition of *Tg*CGL-N360S with the *Tg*CGL monomer
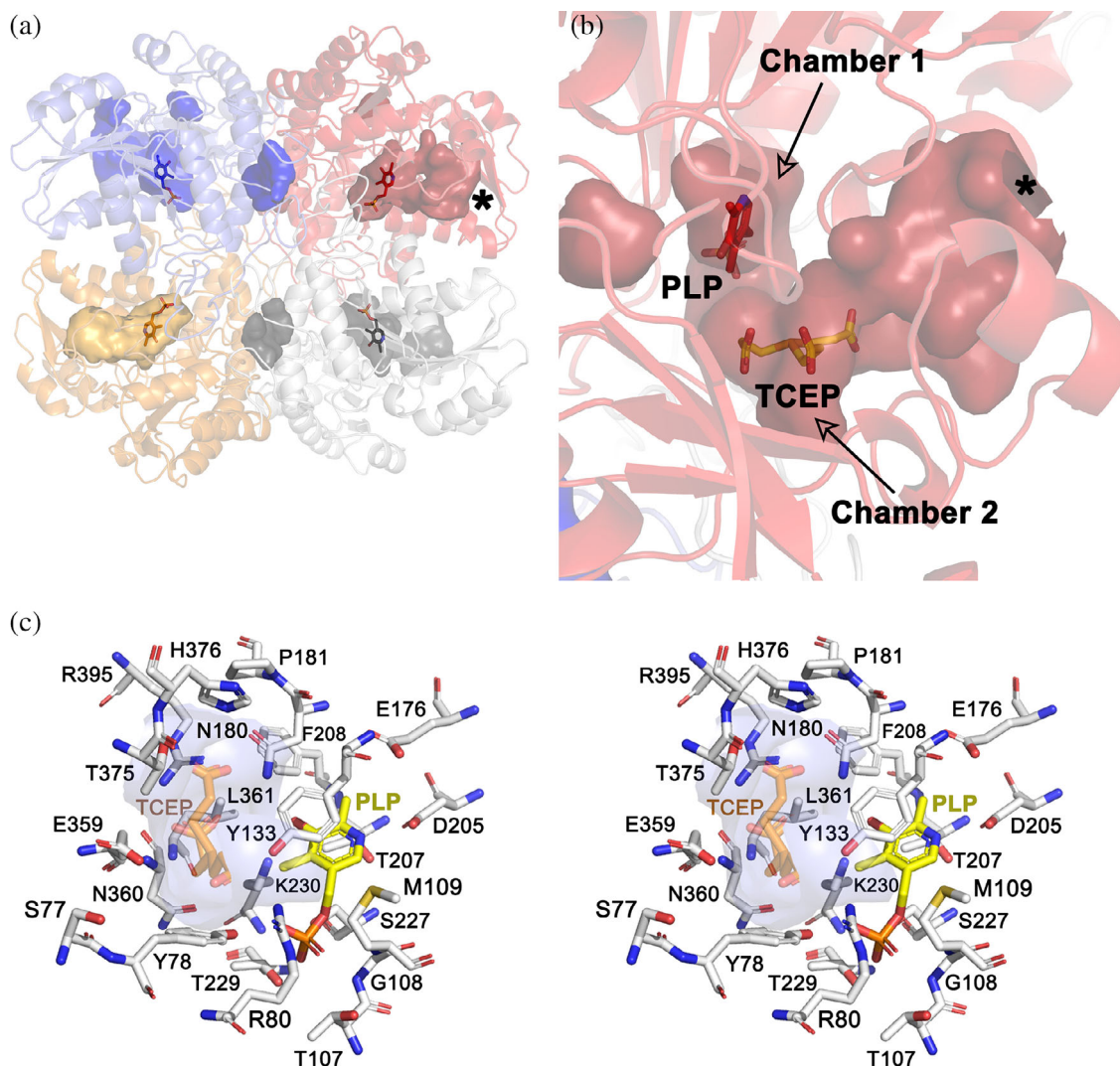
FIGURE 3 *Tg*CGL active site. (a) Surface representation of the four equivalent active site cavities present in the *Tg*CGL tetramer (colored in blue, red, orange, and gray, respectively). One PLP molecule (in sticks) is located at the bottom of each main cleft. The four monomers (in ribbons) are colored distinctly. (b) The main cavity (red surface) of each *Tg*CGL subunit includes two connected chambers. The innermost one harbors a PLP molecule, whereas the precedent cleft, which is directly connected to the solvent (cavity entrance marked with an asterisk) host the first substrate. (c) Stereopair showing the main residues configuring the *Tg*CGL active site cavity. PLP is colored in yellow. Our crystals of wild-type *Tg*CGL revealed a co-crystallized molecule of TCEP (orange sticks) that was present in the crystallization buffer. The semi-transparent blue surface indicates the location of TCEP in chamber 2 of the active site

($rmsd$ = 0.220) and dimer ($rmsd$ = 0.249) revealed some differences in the V351-F393 loop, which appeared slightly open in the mutant enzyme. The most significant displacement of the main chain is observed at residue N378, which is shifted by approximately 4 Å in the mutant (Figure S4).

2.1.2 | *Tg* CGL variants crystallized in presence of Cth

Except for the above-described loop, the superimposition of the crystal structures of native and N360S variants

obtained in the presence of Cth showed no significant differences. However, different molecules were detected within the corresponding catalytic cavities. After careful analysis of refinement outcomes, considering the possible presence of Cth, Cys, or KTB, we concluded that KTB was the substrate that best suited the residual electron density found in the catalytic cavity of wild-type *Tg*CGL, in agreement with the previously reported sole α,γ-elimination capacity (Figure 1, reaction 1) of the native enzyme (Maresi et al., 2018). The carboxylate group of KTB forms a salt bridge with the guanidine group of R395 and H-bonds with the main chain amino group of N360, as well as the amino group of the side

FIGURE 4 *Tg*CGL and *Tg*CGL-N360S enzymes crystallized in the presence of Cth. (a) Main residues of the catalytic site of native *Tg*CGL. The electron density corresponds to a Polder omit map calculated around PLP. The molecule represented in orange sticks is KTB. (b) 2Fo-Fc map around the KTB molecule resulting from the model refinement. (c) Polder omit map calculated around PLP in the *Tg*CGL-N360S mutant. The molecule represented in salmon sticks is HCys. (d) 2Fo-Fc map centered on the HCys molecule after the model refinement. (e) Analysis of dansylated products using reverse phase HPLC. Pure standard Cth, Cys and HCys (top) and products obtained following a 1 h incubation of wild-type *Tg*CGL (middle) or *Tg*CGL-N360S (bottom) with Cth
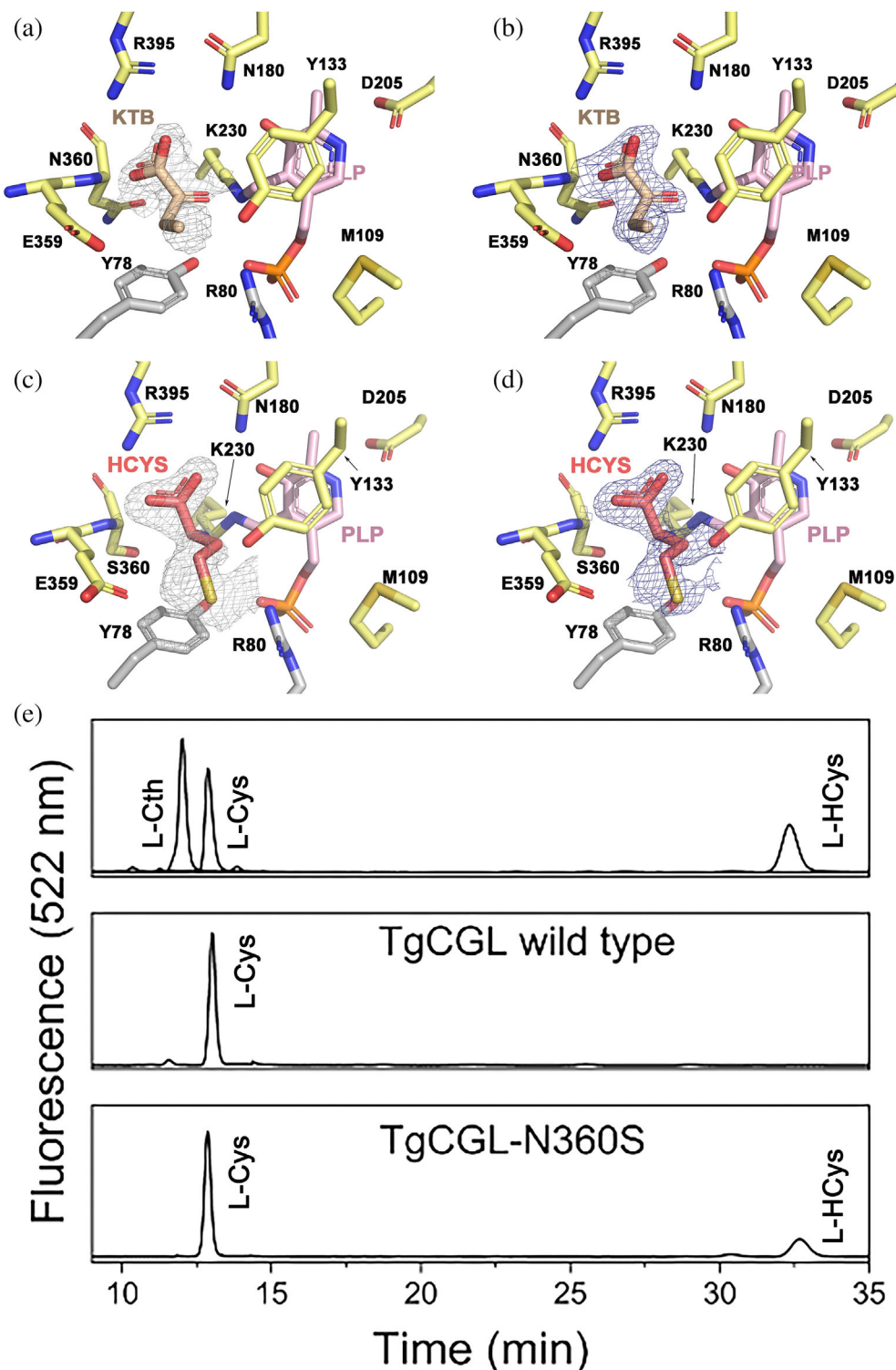
chain of N180 (Figure 4a,b). The carbonyl moiety of KTB is oriented toward the internal aldimine formed by K230 and PLP, and in turn, interacts via an H-bond with the hydroxyl group of Y133. The methyl group of KTB is exposed to the wider pocket of the catalytic site.

On the other hand, HCys, the product of the α, β-elimination (Figure 1, reaction 3), was found in the

catalytic cavity of *Tg*CGL-N360S (Figure 4c,d). HCys forms a salt link with R395 through its carboxylate group and interacts with the side chain of N180 and with the main chain of S360. The amino group of HCys is oriented toward the amino group of K230, which is covalently linked to PLP, forming an internal aldimine. The amino group of HCys is also at the H-bond distance (2.8 Å) of

the hydroxyl of Y133. Finally, the thiol of HCys participates in H-bonds with E359, Y133, and R80 of the adjacent monomer.

The ability of wild-type and N360S variant to catalyze the α,γ- and α,β-elimination reactions, respectively was further analyzed by reverse phase high-performance liquid chromatography (HPLC). This method provides a useful tool for analyzing the products of the TgCGL-catalyzed reactions (Conter et al., 2020). Cys was the only product detected following incubation of wild-type TgCGL with Cth, confirming that the enzyme is proficient at catalyzing the α,γ-elimination (Figure 4e). The enzyme does not catalyze the β-elimination of Cth as HCys was not detected in the chromatogram. On the other hand, incubation of the N360S variant with Cth generates a prominent absorbance peak corresponding to Cys and a minor peak corresponding to HCys, confirming the ability of the mutant enzyme to catalyze both α,γ- and α,β-elimination reactions (Figure 4e).

Previous modeling studies on TgCGL hypothesized that the long side chain of N360 might interfere with an appropriate orientation of the sulfur atom at the γ-position with respect to the PLP molecule to perform the β-cleavage of Cth (Maresi et al., 2018). However, the structures of native and TgCGL-N360S have shown that the side chains of both N360 (in the native enzyme), or its S360 equivalent (in the variant), are not oriented toward the catalytic site, making steric hindrance between the sulfur atom of Cth and the amide group of aspartate (or the hydroxyl group of serine) unlikely.

Our structures suggested that TgCGL selectivity might be encountered by a reduction in the volume of the catalytic cavity (from 287 Å^3 in the native enzyme to 152 Å^3 in the N360S variant), caused by a conformational displacement of loop L351-393 toward helix α4 in the mutant. However, despite a reduction in volume, the N360S mutant still retains the ability to perform the α,γ-elimination reaction. A detailed comparison of the catalytic cavities of the CGLs whose structure is known (performed with CASTp server; Tian et al., 2018), with enzymes that exclusively perform the β-elimination reaction (e.g., Escherichia coli CBL), led us conclude that the volume of the catalytic cavity of TgCGL-N360S (capable of cleaving both the CγS bond and the CβS bond of Cth) is in the range of the E. coli CBL enzyme (152 Å^3 in both cases; Figure S5). Likewise, we found that the CGL enzymes from L. plantarum and yeast (which also catalyze γ- and β-cleavage; Hopwood et al., 2014; Matoba et al., 2020), exhibit a similar available volume (146 and 148 Å^3, respectively). According to this approximation one would expect that both native TgCGL and HsCGL, that only perform γ-cleavage, would display larger catalytic sites. Native TgCGL accomplishes this hypothesis

(288 Å^3), but not HsCGL, which shows a reduced volume (87 Å^3).

Searching for alternative explanations, other authors have proposed that the reaction specificity of CGLs depends on a pair of highly conserved glutamate residues (E59-E339 in HsCGL, and E48-E333 in yeast CGL, respectively; Hopwood et al., 2014; Messerschmidt et al., 2003), which are located at the entrance of the active site and coordinate the cysteinyl moiety of Cth, providing a negatively charged surface. Interestingly, the equivalent glutamate in TgCGL (E359) is conserved and stabilizes the thiol group of the HCys product obtained after β-elimination of Cth, as shown in the crystal structure of TgCGL-N360S (Figure 4c,d), suggesting that, as observed in yeast, E359 is key in determining the orientation of the sulfur atom of Cth within the catalytic cavity of TgCGL. Residue E48 also plays a critical role in the active site of the yeast enzyme. In toxoplasma, however, the equivalent glutamate is replaced by S77. Moreover, S77 participates in an H-bond network involving residues E359, T81, and R80, thus helping to orient E359 within the cavity. Unfortunately, despite significant experimental efforts, we failed to crystallize the TgCGL-S77E mutant. One possible explanation for this failure is the potential destabilization of the overall structure caused by the mutation, as postulated in (Maresi et al., 2018). Notably, the replacement of S77 by glutamate completely abolished the enzyme activity toward Cth (Maresi et al., 2018).

Using the yeast enzyme, Hopwood et al. proposed that residues E333 and L335 flanking S334 have a relevant role in fixing the final orientation of the catalytic K203 that binds PLP (Figure S5). According to their model, the specificity of the CGL reactions is mediated by interactions that optimize the relative positions of the substrate, the PLP, and the lysine (Hopwood et al., 2014). In this regard, a mutational study on E. coli CGS, an enzyme belonging to the fold type I family of PLP-dependent enzymes, revealed that substitutions at S326 (N360 in T. gondii) have a key role in guiding the ε-amino group of catalytic lysine (K198) (Jaworski et al., 2012). Our TgCGL structures show that the N360S mutation increases the distance between the nitrogen of K230 and the oxygen of the asparagine and serine side chain, respectively (from 4.6 to 5.2 Å). This difference might modulate the electronic properties of PLP, allowing or restricting the access of the catalytic base to the C4′ and Cβ positions of the PLP and substrate, respectively.

2.2 | Crystal structure of TgCGL-N360S in complex with Cys

It was reported that the addition of Cys could inhibit CGL from the α,γ-elimination reaction (Cherest
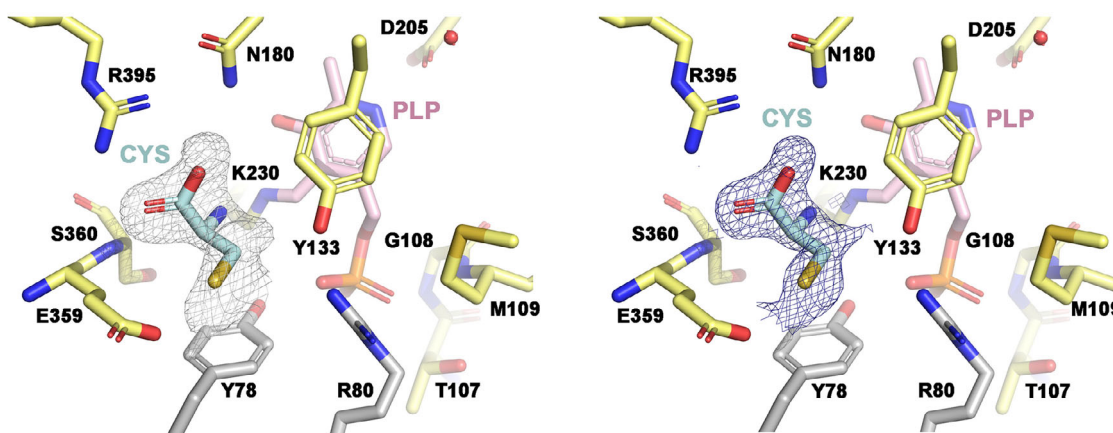
FIGURE 5 Catalytic site of *Tg*CGL-N360S co-crystallized with Cys. Polder omit map (left) and 2Fo-Fc electron density map (right) calculated around the location of the Cys molecule

et al., 1993; Huang et al., 2010; Maresi et al., 2018; Sun et al., 2009; Yamagata et al., 2002). However, the actual inhibitory mechanism remains poorly understood. Two hypotheses have been postulated (Hopwood et al., 2014; Steegborn et al., 1999; Sun et al., 2009; Yamagata et al., 2002). In humans, the addition of Cys results in the detachment of the PLP cofactor from the enzyme (Sun et al., 2009). This loss is detected spectroscopically by the concomitant disappearance of the absorption peak at 427 nm corresponding to the holoenzyme. However, upon the addition of PLP, holoenzyme can be regenerated. The second hypothesis suggests that Cys interacts with the enzyme forming a cyclic thiazolidine complex (Yamagata et al., 2002). To further understand these findings, we co-crystallized *Tg*CGL, both native and N360S variants, with an excess of Cys. Despite numerous attempts, only crystals of the *Tg*CGL-N360S-Cys complex were obtained at 1.9 Å resolution (Figure 5).

Incubation of *Tg*CGL-N360S with Cys resulted in neither loss of the PLP nor the formation of the cyclic thiazolidine intermediate. We found a stable holoenzyme-Cys complex, in which the K230 remains covalently attached to C4′ of PLP and the Cys molecule is placed nearby the catalytic lysine (Figure 5). The carboxylate group of Cys forms a salt bridge with R395, and an H-bond with the amide group of N180 and the sulfhydryl group of Cys is anchored by an H-bond interaction with E359. Our findings suggest that Cys′ inhibition originates from the sites′ competitive occupation to which other reactive molecules need access for catalysis to continue. Interestingly, the crystal structure of *L. plantarum* CGL (*Lp*CGL) complexed with serine (structural analog of Cys; Figure S5) suggested that the formation of an H-bond between the hydroxyl group of residue Y97 (Y133 in *Tg*CGL) and the Oγ atom of serine (Sγ in Cys) is key in orienting the serine appropriately for the β-elimination

reaction (Matoba et al., 2020). By a similar rationale, it would be expected that to perform the β-elimination of Cys, the thiol group of Cys should interact with residue Y133 in *Tg*CGL. However, in our crystals, Cys adopts an orientation that a priori is not suitable for the β-elimination reaction due to the presence of residue E359 that alternatively interacts with the —SH group of Cys and inhibits the contact between the thiol group of the substrate and Y133. Of note, the E339V variant increases the hydrophobicity of the catalytic site of *Hs*CGL and enhances the binding of Cys within the cavity (PDB ID 5EIG; Cramer et al., 2017). The structural comparison of *Tg*CGL-N360S with *Hs*CGL-E339V has allowed us to confirm that the orientation of Cys within the catalytic site is very similar (Figure S6). Intriguingly, Cys forms an external aldimine in the human enzyme, whereas it is not covalently linked to either the cofactor or the protein in the *Tg*CGL-N360S crystals.

2.3 | Crystal structure of *Tg*CGL variants in complex with PPG

PPG is one of the most used agents to inhibit CGLs (Asimakopoulou et al., 2013). We first characterized the potency of PPG to inhibit the α,γ-elimination activity of wild-type *Tg*CGL and its N360S variant by analyzing the effect of PPG on the formation of Cys using the above-described HPLC approach. The half maximal inhibitory concentration (IC$_{50}$) of PPG was determined as 20 ± 4 μM for wild-type *Tg*CGL and 0.6 ± 0.1 μM for *Tg*CGL-N360S, respectively (Figure 6a).

To understand the mechanism underlying the effect of PPG on *Tg*CGL, we next determined the crystal structure of the *Tg*CGL-PPG complex, both for the native (Table S1) and the mutant (Table S2) protein constructs.
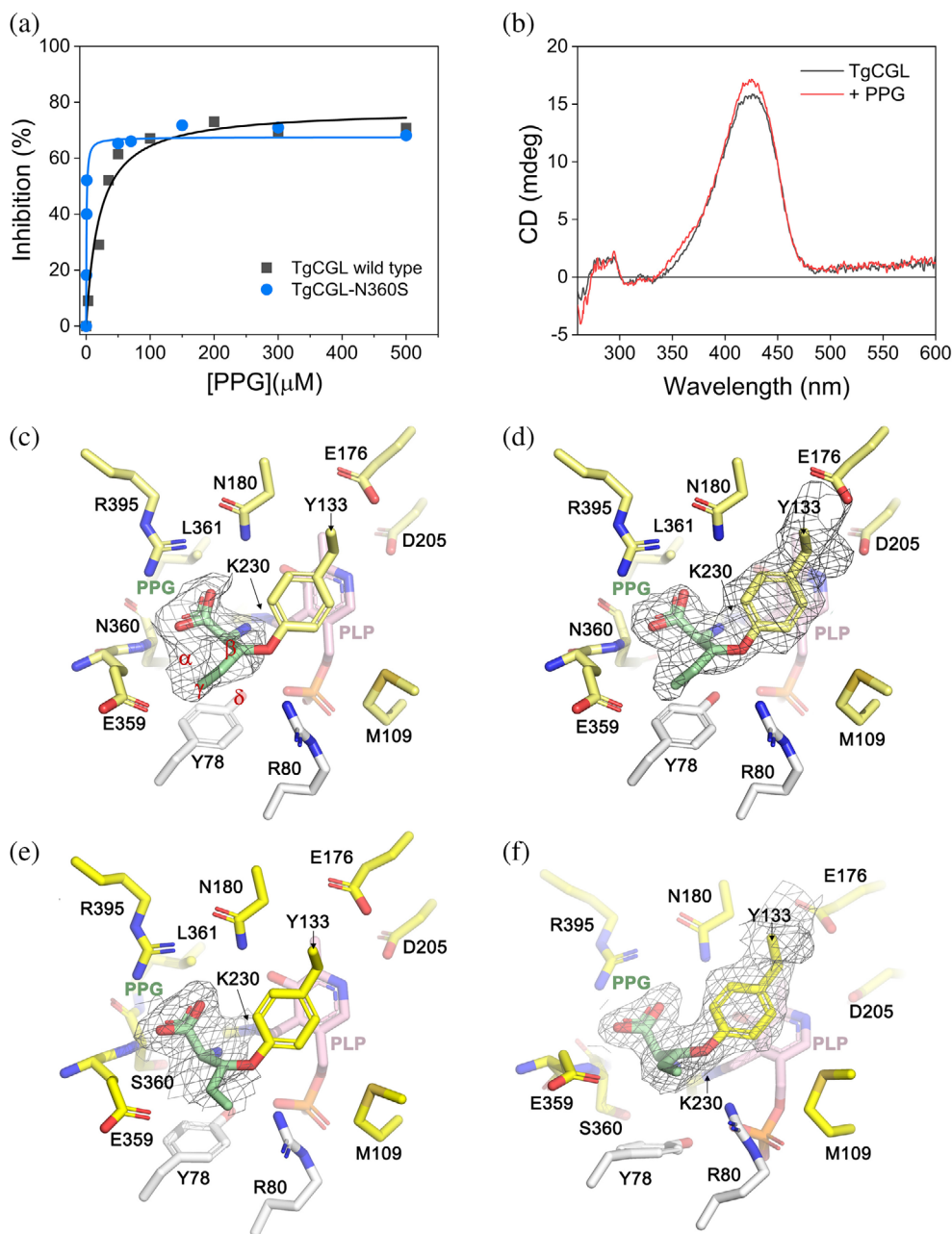
FIGURE 6 *Tg*CGL co-crystallized with PPG. (a) *In vitro* PPG inhibition on *Tg*CGL. Representative graph of percentage inhibition against concentration of PPG in the presence of 8 mM L-Cth substrate. (b) CD spectra of 1 mg/mL *Tg*CGL alone and upon addition of 0.5 mM D,L-propargylglycine (PPG). (c–f) Main residues within the catalytic site of *Tg*CGL. (c) Polder omit map of native *Tg*CGL. (d) 2Fo-Fc map, calculated from the last round of refinement of native *Tg*CGL with PPG (green sticks). (e) Polder omit map of *Tg*CGL-N360S with the PPG calculated within a sphere of 2.6 Å around the inhibitor. (f) 2Fo-Fc map calculated from the last round of refinement of *Tg*CGL-N360S bound to PPG. The position of the C-atoms in PPG is highlighted in red Greek letters. PPG is transformed in its vinyl ether in all cases (see Figure 7)

We found that in the crystal structure of wild-type *Tg*CGL-PPG complex, the residue K230 remains covalently bound to the PLP, forming the internal aldimine, and the PPG molecule, though it is located nearby, does not covalently bind the catalytic lysine (Figure 6c,d). Interestingly, the carboxylate group of the inhibitor points to residue E359, leading the Cβ of PPG to bind covalently to the hydroxyl group of Y133. Moreover, the amino group of PPG is near (2.7 Å) and oriented toward the internal aldimine formed by K230 and PLP.

The crystal structure of the *Tg*CGL-N360S-PPG complex showed a different orientation of the inhibitor within the cavity (Figure 6e,f). The Cβ atom of PPG appears close to Y133 (1.4 Å), suggesting a putative bond,

while PPG again seems to form a vinyl ether. In contrast to the native enzyme, in the mutant, the double bond of PPG is oriented to residue R80 of the adjacent monomer. The side chains of R395 and N180 and the backbone of S360 are H-bonded to the carboxylate group of PPG. Finally, the amino group linked to the Cα atom of PPG interacts with the hydroxyl group of Y133 (at 2.4 Å) and points toward the internal aldimine of the enzyme (at 3.5 Å).

From the above analysis of PPG enzyme complexes, we identified seven residues that interact with PPG: R395, Y133, N/S360, K230, N180, R80 (of the adjacent subunit), and E359 (Figure 6c–f). Interestingly, E359 may be crucial for specific inhibitor design since it is
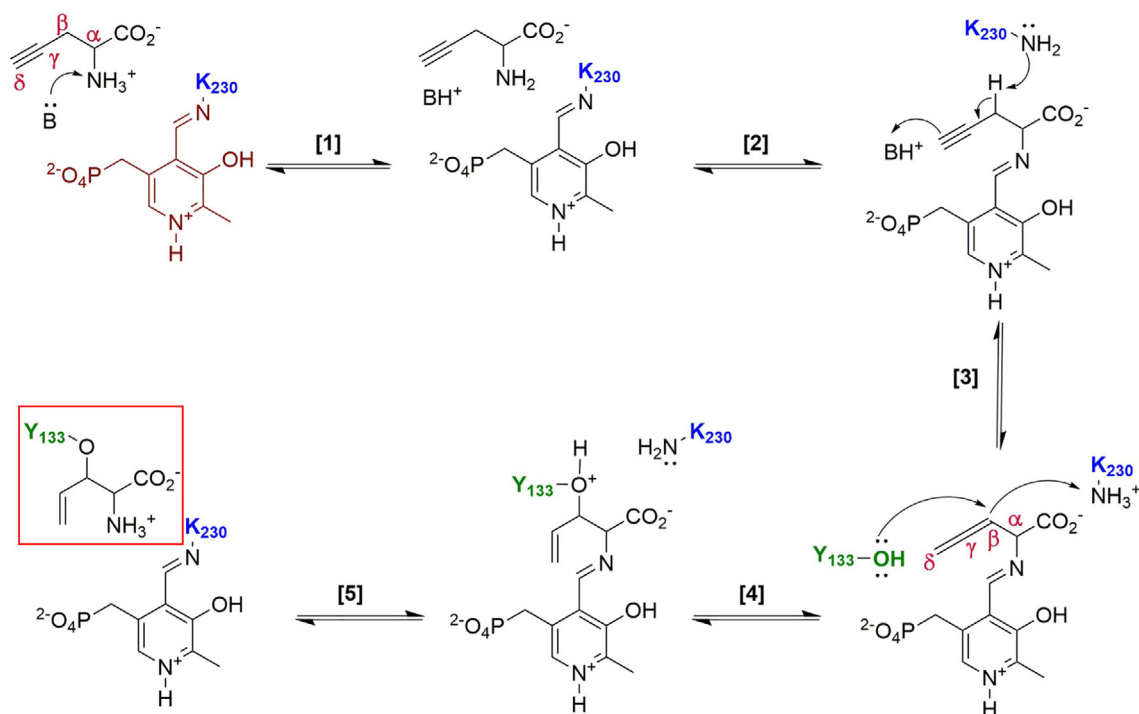
FIGURE 7 Mechanism of inhibition of *Tg*CGL by D,L-propargylglycine (PPG). The PPG is deprotonated by the R80 of the adjacent monomer (step 1) for transaldimination to occur (step 2). Residue K230 attracts the proton at β-position of alkyne to form the allene intermediate (step 3). The hydroxyl group of Y133 attacks the β-position of the allene to generate the vinyl ether (step 4). The internal aldimine is regenerated and Y133 is covalently bound to vinylether of PPG

conserved only in CGL proteins. To date, three crystal structures of PPG-protein complexes have been reported, that is, *Hs*CGL (PDB ID 3COG; Sun et al., 2009; Figure S7A), methionine γ-lyase (MGL) from *Trichomonas vaginalis* (PDB ID 1E5E; Figure S7B), CsdB lyase from *E. coli* (PDB ID 1I29; Mihara et al., 2002; Figure S7C). These three proteins share with *Tg*CGL the folding of type I PLP enzymes and thus have a very similar catalytic site architecture. In MGL and CsdB, PPG molecules are identical in orientation and both amino groups of PPG are covalently bound to C4′ of PLP, forming an external aldimine (Figure S7). Notably, the hydroxyl group of Y114 in *Hs*CGL and Y111 in MGL is at covalent bond distance of the Cγ atom of PPG (Figure S7A,B). However, in the CsdB structure, the equivalent residue of Y114 (H123) is not covalently bound to Cγ of PPG and is not within proximity for covalent bond formation (Figure S7C). Interestingly, in *Tg*CGL, the Cβ of PPG is covalently bound to Y133 (Figure 6f).

These results prompted us to propose a specific mechanism for the PPG inhibition of the parasitic enzyme (Figure 7). First, the amino group of PPG is deprotonated by a basic residue in the active site for transaldimination to occur (step 2). Next, the β position of the alkyne is deprotonated by K230 to generate the allene intermediate

(step 3), which then undergoes nucleophilic attack by another base (step 4) to form the vinyl ether.

Based on the *Tg*CGL-PPG complex crystal structures, we proposed that the basic amino acid responsible for deprotonation of the incoming PPG (step 1) and protonation of the alkyne (step 3) is R80 of the adjacent monomer. R80 is located at the inhibitor/substrate binding site entrance and is in a favorable position to deprotonate the incoming substrate/inhibitor. In addition, the side chain of R80 is at a distance that facilitates the protonation of the alkyne at the γ position (4.3 and 3.8 Å for the native and mutant *Tg*CGL, respectively; step 3). Importantly, our structures suggest that the hydroxyl group of Y133 serves as the base in step 4 to convert the activated allene to a vinyl ether, forming a covalent bond with the Cβ of the allene, since the Cβ is placed in a favorable position for the nucleophilic attack of Y133. In contrast, in the human enzyme, where the Cγ of PPG is covalently bound to Y114, a proton from the hydroxyl group of Y114 may move to the Cδ atom in PPG, resulting in the formation of an allene derivative. Then, the deprotonated hydroxyl nucleophilically attacks the Cγ atom of the derivative. Importantly, the allenes have an exceptional reactivity, and all three carbon atoms can be attacked, being kinetically and thermodynamically favorable processes (Vitkovskaya et al., 2017). Of note, we found no changes

in the spectral properties of *Tg*CGL after adding PPG (Figure 6b). This is consistent with step 5 of our proposed mechanism, in which the internal aldimine is regenerated, and Y133 is covalently bound to the vinyl ether of PPG. The bound PPG occupies the binding space of the substrate, thus inhibiting *Tg*CGL by blocking access to the catalytic site. In addition, the release of the substrate is prevented due to the covalent bond of PPG to Y133, a key residue in the catalytic process (Clausen et al., 1998; Matoba et al., 2020).

3 | CONCLUSIONS

The transsulfuration pathway plays a central role in cell sulfur metabolism and redox regulation. Different studies have underlined the therapeutic potential of inhibiting the activity of the transsulfuration enzymes in the treatment of pathogenic infections (Bandyopadhyay et al., 2022; Gobert et al., 2019; Marciano et al., 2012; Shatalin et al., 2011, 2021). Knowledge of the three-dimensional structure of these therapeutically relevant targets is crucial to guide the design of new drugs. Herein, we successfully determined the crystal structures of *Tg*CGL and its N360S variant and revealed the residues involved in cofactor, substrates, and PPG binding. In particular, the structural analysis has highlighted the importance of Y133 and its unique specific covalent interaction with PPG, raising a mechanistic hypothesis of PPG-dependent inhibition of *Tg*CGL.

Our structural data can be utilized as a resource for the structure-based design of novel inhibitors of *Tg*CGL to aid in the development of therapies against toxoplasmosis as well as provide significant insights on the structural evolution of CGLs across different organisms.

4 | MATERIALS AND METHODS

4.1 | Proteins production

Wild-type *Tg*CGL and *Tg*CGL-N360S mutant were purified as His-tag proteins as previously described (Maresi et al., 2018) and the homogeneity and purity of enzyme (>95%) was confirmed by SDS/PAGE. The oligomeric state of the proteins was determined by gel filtration analysis employing a GE Healthcare Superdex 200 10/300 GL column in 20 mM sodium phosphate buffer pH 8, 150 mM NaCl and 0.1 mM DTT as described elsewhere (Allegrini et al., 2017; Astegno et al., 2017). The calibration curve was obtained as described (Astegno, Allegrini, et al., 2015; Astegno, Capitani, & Dominici, 2015).

4.2 | Protein crystallization

For crystallization, the enzymes were buffer exchanged into 50 mM HEPES, 150 mM NaCl, 0.1 mM DTT pH 8.0. The crystallization trials were carried out by the vapor-diffusion technique in a sitting drop format following a protocol similar to Fernández-Rodríguez et al. (2021). Droplets were arranged automatically with a MOS-QUITO nanodispenser (SPTLabtech) in 96-well MRC crystallization plates (Molecular Dimensions) containing 200 nL of protein solution mixed with 200 nL of precipitant solution and incubated at 293 K.

The best crystals of wild-type *Tg*CGL were grown in hanging drop in 12% (wt/vol) PEG 3350, 0.1 M sodium citrate pH 4.6 using either CYMAL-3, CYMAL-4, n-nonyl-B-D-maltoside or n-octyl-B-D-thiomaltoside detergents (Hampton Research) at a protein concentration of 20 mg/mL and an approximate time of 72 h. The drops contained 1 μL of protein, 0.8 μL of precipitant and 0.2 μL of detergent. The crystals were collected with nylon loops and frozen after prior immersion in a solution containing 12% (wt/vol) PEG 3350, 0.1 M sodium citrate pH 4.6 and 26% (vol/vol) glycerol as cryoprotective agent. The crystal structure of *Tg*CGL-N360S was obtained after 1–2 days in 12% (wt/vol) PEG 3350, 0.1 M sodium citrate pH 4.6 and 0.2 μL of CYMAL-4 detergent (Hampton Research). Drops consisted of 1 μL of protein solution (10 mg/mL), 0.8 μL of reservoir solution and 0.2 μL detergent. Single *Tg*CGL -N360S crystals were transferred into a cryoprotection solution containing the crystallization buffer with 26% (vol/vol) glycerol and flash frozen in liquid nitrogen.

The enzyme variants were also co-crystallized in the presence of Cys (Sigma-Merck, 168149), Cth (Sigma-Merck, C7505) and PPG (Sigma-Merck, P7888). In all cases, the enzyme variants were aliquoted and independently incubated with ligands in a ratio (1:100) that ensured full occupancy of ligands in the catalytic site of the protein. Crystals of ligand-protein complex appeared after 3 days at 291 K by hanging drop vapor diffusion in 24-well plates, except for the wild-type *Tg*CGL-Cys complex for which no crystals were obtained. The volume of the reservoir was 500 μL and was composed by 12% (wt/vol) PEG 3350, 0.1 M sodium citrate pH 4.6 and CYMAL-3 (when Cys and Cth were used as ligands) or CYMAL-4 (in the case of PPG) as a detergent. Drops were composed by 1 μL of protein solution (15 mg/mL) incubated with 24 and 30 mM of Cth and PPG respectively, 0.8 μL of precipitant and 0.2 μL of detergent. Single crystals were transferred to a cryoprotection solution (crystallization buffer with 27% [vol/vol] glycerol) and flash frozen in liquid N_2.

4.3 | Structural determination by X-ray crystallography

All X-rays datasets were collected at Synchrotron beamlines XALOC (ALBA), and I03/I24 (DIAMOND, UK). The diffraction data were indexed, integrated, and scaled using XDS (Kabsch, 2010) programs. The plots of the self-rotation function were calculated with MOLREP (Vagin & Teplyakov, 2010) and autoPROC three-dimensional structure of *Tg*CGL wild type and mutant alone and in presence of ligands were determined by MR method with PHASER (McCoy et al., 2007) from PHENIX (Adams et al., 2011) using the structure of *Hs*CGL holoenzyme (PDB ID code 2NMP). Ligands geometry restraints builder and optimization was generated with elBOW (Moriarty et al., 2009). Model was built with Coot (Emsley et al., 2010). Figures were done with Pymol (The PyMOL Molecular Graphics System, Version 2.2.3, Schrödinger, LLC) and UCSF Chimera (Pettersen et al., 2004; version 1.13.1; http://www.rbvi.ucsf.edu/chimera). The crystal characteristics and refinement statistics for wild-type *Tg*CGL and *Tg*CGL -N360S are in Tables S1 and S2, respectively.

4.4 | High-performance liquid chromatography

The production of Cys and HCys generated upon α,γ- and α,β-elimination of Cth, respectively was analyzed through reverse phase HPLC (Conter et al., 2020). A 500 μL reaction mixture containing 0.1–8 mM Cth and 30 μM enzyme variants in 50 mM HEPES pH 8.0 was incubated at 37°C for 60 min. Where indicated 0.05–0.5 mM PPG was incubated with the enzyme for 30 min at 25°C. The enzyme was removed from the reaction mixture by centrifugation using a Vivaspin Turbo centrifugal concentrator (10 kDa cutoff, Sartorius). Dansyl chloride (stock 1.5 mg/mL in acetonitrile) was then reacted with the amino acids in the filtered solution following the protocol in Mothersole and Wolthers (2019) and Tapuhi et al. (1981). Following a 30-min incubation at 25°C, the reaction was quenched with 30 μL of pyridine 4% and 20 μL of the mixture was injected onto a C-18 column (Agilent Poroshell 120 HPH RP-C18, 4 μm, 4.6 × 250 mm). The dansylated products were eluted at a flow rate of 1 mL/min at 40°C with a mobile phase of 33.25/66.75 (vol/vol) methanol/water containing 0.008% (vol/vol) triethylamine and 0.6% (vol/vol) glacial acetic acid. The fluorescence detector was set at 335 and 522 nm for excitation and emission wavelengths, respectively.

4.5 | Spectroscopic measurements

CD spectra were recorded on CD spectropolarimeter (Jasco J-1500), equipped with a Peltier-type temperature controller, as previously described (Dindo et al., 2020; Pedretti et al., 2020). Briefly, near UV–Vis (250–600 nm) spectra of 1 mg/mL *Tg*CGL were collected in 1-cm path length quartz cuvette at a scan speed of 50 nm/min in 20 mM sodium phosphate pH 8 at 25°C. A minimum of three accumulations were made for each scan, averaged, and corrected for the blank solution of corresponding buffer (Bombardi et al., 2020).

CONFLICT OF INTEREST STATEMENT

The authors declare no conflict of interest.

ORCID

Carolina Conter https://orcid.org/0000-0002-5999-8667
Alessandra Astegno https://orcid.org/0000-0002-7341-0970
Luis Alfonso Martínez-Cruz https://orcid.org/0000-0002-5856-9377

REFERENCES

Adams PD, Afonine PV, Bunkóczi G, Chen VB, Echols N, Headd JJ, et al. The Phenix software for automated determination of macromolecular structures. Methods (San Diego, Calif). 2011;55:94–106.

Allegrini A, Astegno A, La Verde V, Dominici P. Characterization of C-S lyase from *Lactobacillus delbrueckii* subsp. bulgaricus ATCC BAA-365 and its potential role in food flavour applications. J Biochem. 2017;161:349–60.

Asimakopoulou A, Panopoulos P, Chasapis CT, Coletta C, Zhou Z, Cirino G, et al. Selectivity of commonly used pharmacological inhibitors for cystathionine β synthase (CBS) and cystathionine γ lyase (CSE). Br J Pharmacol. 2013;169:922–32.

Astegno A, Allegrini A, Piccoli S, Giorgetti A, Dominici P. Role of active-site residues Tyr55 and Tyr114 in catalysis and substrate specificity of *Corynebacterium diphtheriae* C-S lyase. Proteins. 2015;83:78–90.

Astegno A, Capitani G, Dominici P. Functional roles of the hexamer organization of plant glutamate decarboxylase. Biochim Biophys Acta. 2015;1854:1229–37.

Astegno A, Maresi E, Bertoldi M, La Verde V, Paiardini A, Dominici P. Unique substrate specificity of ornithine aminotransferase from *Toxoplasma gondii*. Biochem J. 2017;474:939–55.

Bandyopadhyay P, Pramanick I, Biswas R, Ps S, Sreedharan S, Singh S, et al. S-Adenosylmethionine-responsive cystathionine β-synthase modulates sulfur metabolism and redox balance in *Mycobacterium tuberculosis*. Sci Adv. 2022;8:eabo0097.

Bombardi L, Pedretti M, Conter C, Dominici P, Astegno A. Distinct calcium binding and structural properties of two centrin isoforms from *Toxoplasma gondii*. Biomolecules. 2020;10:1142.

Cherest H, Thomas D, Surdin-Kerjan Y. Cysteine biosynthesis in Saccharomyces cerevisiae occurs through the transsulfuration pathway which has been built up by enzyme recruitment. J Bacteriol. 1993;175:5366–74.

Clausen T, Huber R, Prade L, Wahl MC, Messerschmidt A. Crystal structure of *Escherichia coli* cystathionine gamma-synthase at 1.5 a resolution. EMBO J. 1998;17:6827–38.

Conter C, Fruncillo S, Favretto F, Fernández-Rodríguez C, Dominici P, Martínez-Cruz LA, et al. Insights into domain organization and regulatory mechanism of cystathionine beta-synthase from *Toxoplasma gondii*. Int J Mol Sci. 2022;23:8169.

Conter C, Fruncillo S, Fernández-Rodríguez C, Martínez-Cruz LA, Dominici P, Astegno A. Cystathionine β-synthase is involved in cysteine biosynthesis and H(2)S generation in *Toxoplasma gondii*. Sci Rep. 2020;10:14657.

Cramer SL, Saha A, Liu J, Tadi S, Tiziani S, Yan W, et al. Systemic depletion of L-cyst(e)ine with cyst(e)inase increases reactive oxygen species and suppresses tumor growth. Nat Med. 2017; 23:120–7.

Dindo M, Mandrile G, Conter C, Montone R, Giachino D, Pelle A, et al. The ILE56 mutation on different genetic backgrounds of alanine:glyoxylate aminotransferase: clinical features and biochemical characterization. Mol Genet Metab. 2020;131:171–80.

Emsley P, Lohkamp B, Scott WG, Cowtan K. Features and development of Coot. Acta Crystallogr D Biol Crystallogr. 2010;66:486–501.

Fernández-Rodríguez C, Oyenarte I, Conter C, González-Recio I, Núñez-Franco R, Gil-Pitarch C, et al. Structural insight into the unique conformation of cystathionine β-synthase from *Toxoplasma gondii*. Comput Struct Biotechnol J. 2021;19:3542–55.

Gobert AP, Latour YL, Asim M, Finley JL, Verriere TG, Barry DP, et al. Bacterial pathogens hijack the innate immune response by activation of the reverse transsulfuration pathway. MBio. 2019;10:e02174-19.

González-Recio I, Fernández-Rodríguez C, Simón J, Goikoetxea-Usandizaga N, Martínez-Chantar ML, Astegno A, et al. Current structural knowledge on cystathionine β-synthase, a pivotal enzyme in the Transsulfuration pathway. (2020). In eLS, John Wiley & Sons, Ltd (Ed.). https://doi.org/10.1002/9780470015902.a0028966

Hopwood EM, Ahmed D, Aitken SM. A role for glutamate-333 of *Saccharomyces cerevisiae* cystathionine gamma-lyase as a determinant of specificity. Biochim Biophys Acta. 2014;1844:465–72.

Huang S, Chua JH, Yew WS, Sivaraman J, Moore PK, Tan CH, et al. Site-directed mutagenesis on human cystathionine-gamma-lyase reveals insights into the modulation of H$_2$S production. J Mol Biol. 2010;396:708–18.

Jaworski AF, Lodha PH, Manders AL, Aitken SM. Exploration of the active site of *Escherichia coli* cystathionine γ-synthase. Protein Sci. 2012;21:1662–71.

Kabsch W. XDS. Acta Crystallogr D Biol Crystallogr. 2010;66:125–32.

Kobylarz MJ, Grigg JC, Liu Y, Lee MSF, Heinrichs DE, Murphy MEP. Deciphering the substrate specificity of SbnA, the enzyme catalyzing the first step in Staphyloferrin B biosynthesis. Biochemistry. 2016;55:927–39.

Krissinel E, Henrick K. Detection of protein assemblies in crystals. In Berthold MR, Glen RC, Diederichs K, Kohlbacher O, Fischer I, editors. Computational life sciences. CompLife. Springer Berlin Heidelberg. 2005. Lecture Notes in Computer Science(), vol 3695. Springer, Berlin, Heidelberg. https://doi.org/10.1007/11560500_15

Lee D, Jeong S, Ahn J, Ha N-C, Kwon A-R. Crystal structure of bacterial cystathionine Γ-Lyase in the cysteine biosynthesis pathway of *Staphylococcus aureus*. Crystals. 2019;9:656.

Marciano D, Santana M, Nowicki C. Functional characterization of enzymes involved in cysteine biosynthesis and H2S production in *Trypanosoma cruzi*. Mol Biochem Parasitol. 2012;185:114–20.

Maresi E, Janson G, Fruncillo S, Paiardini A, Vallone R, Dominici P, et al. Functional characterization and structure-

guided mutational analysis of the transsulfuration enzyme cystathionine γ-Lyase from *Toxoplasma gondii*. Int J Mol Sci. 2018;19:2111.

Matoba Y, Noda M, Yoshida T, Oda K, Ezumi Y, Yasutake C, et al. Catalytic specificity of the *Lactobacillus plantarum* cystathionine γ-lyase presumed by the crystallographic analysis. Sci Rep. 2020;10:14886.

McCoy AJ, Grosse-Kunstleve RW, Adams PD, Winn MD, Storoni LC, Read RJ. Phaser crystallographic software. J Appl Cryst. 2007;40:658–74.

Messerschmidt A, Worbs M, Steegborn C, Wahl MC, Huber R, Laber B, et al. Determinants of enzymatic specificity in the Cys-met-metabolism PLP-dependent enzymes family: crystal structure of cystathionine gamma-lyase from yeast and intrafamiliar structure comparison. Biol Chem. 2003;384:373–86.

Mihara H, Fujii T, Kato S, Kurihara T, Hata Y, Esaki N. Structure of external aldimine of *Escherichia coli* CsdB, an IscS/NifS homolog: implications for its specificity toward selenocysteine. J Biochem. 2002;131:679–85.

Mironov A, Seregina T, Nagornykh M, Luhachack LG, Korolkova N, Lopes LE, et al. Mechanism of H₂S-mediated protection against oxidative stress in *Escherichia coli*. Proc Natl Acad Sci. 2017;114:6022–7.

Moriarty NW, Grosse-Kunstleve RW, Adams PD. Electronic Ligand Builder and Optimization Workbench (eLBOW): a tool for ligand coordinate and restraint generation. Acta Crystallogr D Biol Crystallogr. 2009;65:1074–80.

Mothersole RG, Wolthers KR. Structural and kinetic insight into the biosynthesis of H₂S and l-Lanthionine from l-cysteine by a pyridoxal l-phosphate-dependent enzyme from *Fusobacterium nucleatum*. Biochemistry. 2019;58:3592–603.

Nagasawa T, Kanzaki H, Yamada H. Cystathionine gamma-lyase of *Streptomyces phaeochromogenes*. The occurrence of cystathionine gamma-lyase in filamentous bacteria and its purification and characterization. J Biol Chem. 1984;259:10393–403.

Nzungize L, Ali MK, Wang X, Huang X, Yang W, Duan X, et al. *Mycobacterium tuberculosis* metC (Rv3340) derived hydrogen sulphide conferring bacteria stress survival. J Drug Target. 2019;27:1004–16.

Oliveira EF, Cerqueira NMFSA, Fernandes PA, Ramos MJ. Mechanism of formation of the internal Aldimine in pyridoxal 5′-phosphate-dependent enzymes. J Am Chem Soc. 2011;133: 15496–505.

Pedretti M, Conter C, Dominici P, Astegno A. SAC3B is a target of CML19, the centrin 2 of *Arabidopsis thaliana*. Biochem J. 2020; 477:173–89.

Pettersen EF, Goddard TD, Huang CC, Couch GS, Greenblatt DM, Meng EC, et al. UCSF chimera—a visualization system for exploratory research and analysis. J Comput Chem. 2004;25: 1605–12.

Sagong H-Y, Kim B, Joo S, Kim K-J. Structural and functional characterization of cystathionine γ-lyase from *Bacillus cereus* ATCC 14579. J Agric Food Chem. 2020;68:15267–74.

Shatalin K, Nuthanakanti A, Kaushik A, Shishov D, Peselis A, Shamovsky I, et al. Inhibitors of bacterial H₂S biogenesis targeting antibiotic resistance and tolerance. Science. 2021;372:1169–75.

Shatalin K, Shatalina E, Mironov A, Nudler E. H2S: a universal defense against antibiotics in bacteria. Science. 2011;334: 986–90.

Steegborn C, Clausen T, Sondermann P, Jacob U, Worbs M, Marinkovic S, et al. Kinetics and inhibition of recombinant human cystathionine gamma-lyase. Toward the rational control of transsulfuration. J Biol Chem. 1999;274:12675–84.

Sun Q, Collins R, Huang S, Holmberg-Schiavone L, Anand GS, Tan C-H, et al. Structural basis for the inhibition mechanism of human cystathionine γ-Lyase, an enzyme responsible for the production of H₂S. J Biol Chem. 2009;284:3076–85.

Tapuhi Y, Schmidt DE, Lindner W, Karger BL. Dansylation of amino acids for high-performance liquid chromatography analysis. Anal Biochem. 1981;115:123–9.

Tian W, Chen C, Lei X, Zhao J, Liang J. CASTp 3.0: computed atlas of surface topography of proteins. Nucleic Acids Res. 2018;46: W363–w7.

Vagin A, Teplyakov A. Molecular replacement with MOLREP. Acta Crystallogr D Biol Crystallogr. 2010;66:22–5.

Vitkovskaya NM, Kobychev VB, Bobkov AS, Orel VB, Schmidt EY, Trofimov BA. Nucleophilic addition of ketones to acetylenes and Allenes: a quantum-chemical insight. J Org Chem. 2017; 82:12467–76.

Wang Y, Chen H, Huang Z, Yang M, Yu H, Peng M, et al. Structural characterization of cystathionine γ-lyase smCSE enables aqueous metal quantum dot biosynthesis. Int J Biol Macromol. 2021;174:42–51.

Wang Z-D, Liu H-H, Ma Z-X, Ma H-Y, Li Z-Y, Yang Z-B, et al. *Toxoplasma gondii* infection in immunocompromised patients: a systematic review and meta-analysis. Front Microbiol. 2017; 8:389.

Yadav PK, Vitvitsky V, Kim H, White A, Cho U-S, Banerjee R. S-3-Carboxypropyl-l-cysteine specifically inhibits cystathionine γ-lyase–dependent hydrogen sulfide synthesis. J Biol Chem. 2019;294:11011–22.

Yamagata S, Isaji M, Yamane T, Iwama T. Substrate Inhibition ofL-Cysteine α,β-Elimination Reaction Catalyzed byL-Cystathionine γ-Lyase ofSaccharomyces cerevisiae. Biosci Biotechnol Biochem. 2002;66:2706–9.

SUPPORTING INFORMATION

Additional supporting information can be found online in the Supporting Information section at the end of this article.